Dynamic Soaring in Finite-Thickness Wind Shears: an Asymptotic Solution

Dynamic Soaring in Finite-Thickness Wind Shears: an Asymptotic Solution

Gabriel D. Bousquet,* Michael S. Triantafyllou,† Jean-Jacques E. Slotine†

Massachusetts Institute of Technology, Cambridge, MA, 02139, USA

Building upon our recent description of dynamic soaring as a succession of small amplitude arcs nearly crosswind, rather than a sequence of half-turns, we formulate an asymptotic expansion for the minimum-wind dynamic soaring cycle when the shear layer between the slow and fast regions has a thin but finite thickness. Our key assumption is that the trajectory remains approximately planar even in finite thickness shears. We obtain an analytical approximation for key flight parameters as a function of the shear layer thickness Δ. In particular we predict that the turn amplitude, maximum climb angle, and cycle altitude scale as $\Delta^{1/5}$, $\Delta^{2/5}$, and $\Delta^{3/5}$, respectively. Our asymptotic expansion is validated against numerical trajectory optimizations and compared with recordings of albatross flights. While the model validity increases with wing loading, it appears to constitute an accurate description down to wing loadings as low as 4kg/m^2 for oceanic boundary layer soaring, a third that of the wandering albatross.

Introduction

Wind energy extraction can be classified into two broad mechanisms. The first one results from an interplay between gravitational forces and upward currents, as in thermal soaring. The second one relies on the homogenization of an non-uniform flow through transfer or momentum between regions of different velocities. This second mechanism is what drives sailboats (momentum is transferred between the wind and the water) and wind turbines (momentum is transferred between the air and the ground). It is also the basic principle of both turbulence soaring and dynamic soaring.[1] In turbulence[2] and dynamic[3] soaring: momentum is transferred between regions of an inhomogeneous wind. In this paper, we focus on a specific type of dynamic soaring: unpowered flight in a deterministic, horizontal, stratified and unidirectional wind field. This framework successfully explains the main mechanism of the albatross' flight:[3–8] they perform dynamic soaring by transferring momentum between the relatively slow layer of air in the first meter above the ocean surface and behind separated waves, and the relatively faster winds higher up at about 10–20 m of altitude.[4,9,10] The albatross gains energy by cyclically maneuvering between the slow and fast layers, periodically pumping momentum out of the wind layer and injecting it into the boundary layer, in a characteristic S-shaped trajectory.

A question that is central to both biologists who study the albatross' ecology and to engineers who want to create albatross-inspired systems is that of whether, in a given wind profile, a given glider is potentially able to sustain flight.

Important conceptual and analytical studies[4,7,8,11] have been performed since Rayleigh's seminal description of dynamic soaring. In the last two decades, significant efforts have been further dedicated to simulating dynamic soaring with models of ever increasing complexity.[5–7,12,13] Combined with recent high accuracy recordings of flying albatrosses,[9,10] these studies have increased our understanding of dynamic soaring, and constitute valuable data to compare theories against.

As we discussed in [1], despite the aforementioned efforts, fundamental aspects of dynamic soaring remain poorly understood. In particular, while a large portion of the literature describes dynamic soaring as a sequence of half-turns connecting upwind climbs and downwind dives through the surface shear layer,[7,8,14–22] observational data as well as simulations show that over the dynamic soaring cycle, the albatross remains

*PhD. Candidate, Department of Mechanical Engineering, AIAA Student Member.

†Professor, Department of Mechanical Engineering.

mostly crosswind at all times and virtually never faces, of flies directly with, the wind. We showed analytically and verified numerically that this distinction is important both conceptually and quantitatively, and suggested that it is fruitful to describe the trajectory of the albatross as a succession of small turns. Given this alternative framework, dynamic soaring energetics is quantitatively similar to that of sailboats. In the thin shear limit, small turns only require two-thirds the wind predicted by previous, half-turn based analytical models.

In this paper we solve the minimum wind problem, asymptotically in the shear layer thickness. Our asymptotic solution is in quantitative agreement with trajectory optimization models, up to a shear thickness of $\sim$20% (cruise speed)$^2/g$, (20% of 22 m for a wandering albatross).

After reviewing our dynamic model and the results of [1] for infinitely thin shears, we solve the minimum wind problem through an asymptotic expansion, valid for small but finite shear thicknesses. The range of validity of the model and its limitations are discussed while it is compared to numerical simulations and recordings of flying albatrosses.

I. Dynamic model

I.A. Equations of motion

Following [1] and citations herein[7,23] we use a 3-degree-of-freedom glider model. Our frame or reference is $(\mathbf{e}_x, \mathbf{e}_y, \mathbf{e}_z) = (\mathbf{e}_{\text{East}}, \mathbf{e}_{\text{North}}, \mathbf{e}_{\text{Up}})$ with $\mathbf{e}_z$ pointing up. The state is (V, ψ, γ, z) where V is the glider airspeed, ψ is the heading angle, *i.e.* the angle between $\mathbf{x}$ and the projection of the airspeed $\mathbf{V}$ in the xy-plane and γ is the climb angle *i.e.* the angle between $\mathbf{V}$ and the xy-plane, positive nose up. We assume the existence of a varying wind $-W(z)\mathbf{e}_y$ (blowing from positive to negative y when $W > 0$). The control inputs $\mathbf{u} = (c_L, \phi)$ are the lift coefficient and bank angle. The equations of motion are:

$$m\dot{V} = -D - mg\sin\gamma + m\dot{W}\cos\gamma\sin\psi \tag{1a}$$

$$mV\dot{\gamma} = L\cos\phi - mg\cos\gamma - m\dot{W}\sin\gamma\sin\psi \tag{1b}$$

$$mV\dot{\psi}\cos\gamma = L\sin\phi + m\dot{W}\cos\psi \tag{1c}$$

$$\dot{z} = V\sin\gamma \tag{1d}$$

We have not included the equations for x, y as they are irrelevent for the minimum wind problem. Lift and drag are specified according to $L, D = 1/2 c_{L,D}\rho S V^2$. We assume quadratic drag $c_D = c_{D,0} + k c_L^2$ with $k^{-1} = 4 f_{\max}^2 c_{D,0}$ where $f_{\max}$ is the glider maximum lift-to-drag ratio.

In order to non-dimensionalize Equation (1), we introduce the following quantities: $V_c = \sqrt{\frac{mg}{\frac{1}{2}\rho S}}$, $\lambda = V_c^2/g$ and $t^* = V_c/g$. In terms of the non-dimensionalized variables $v = V/V_c$, $w = W/V_c$, $\tilde{z} = z/\lambda$, $\tau = t/t^*$ and $(\cdot)' = d/d\tau(\cdot)$, Equation (1) thereby becomes

$$v' = -c_D v^2 - \sin\gamma + w'\cos\gamma\sin\psi \tag{2a}$$

$$v\gamma' = c_L v^2\cos\phi - \cos\gamma - w'\sin\gamma\sin\psi \tag{2b}$$

$$v\cos\gamma\psi' = c_L v^2\sin\phi + w'\cos\psi \tag{2c}$$

$$\tilde{z}' = v\sin\gamma \tag{2d}$$

$$w' = \partial_{\tilde{z}} w \tilde{z}' \tag{2e}$$

Unless indicated otherwise, below we use non-dimensional quantities. Therefore, the $\tilde{}$ symbol on z will be omitted. When solving the equations numerically we use $f_{\max} = 20$ and $c_{L,f_{\max}} = 0.5$. For dimensional quantities, we use $V_c = 14.5$ m/s and $\lambda = 22$ m, typical of a wandering albatross.

I.B. Wind model

In [1], we utilize a logistic wind profile

$$w(z) = \frac{w_0}{1 + \exp -z/\delta} \tag{3}$$

with $z = 0$ at the center of the shear region (Figure 1). It is parameterized by the wind strength w_0 and a shear thickness parameter δ. For $\delta \gg 1$ it becomes a linear shear field, which has been used to model *e.g.*

the wind field of the jet stream. For $\delta \ll 1$, it converges to the two-layer model of Rayleigh $dw/dz = w_0\delta(z)$ (note that we use the roman script δ for the Dirac distribution). For finite values of δ, it can be interpreted as an approximation of the separated wind field behind waves[24] or mountain ridges.

Note that δ is a parameter that expresses the shear thickness *for the particular parameterization of Equation (3)*. In order to extend our analysis to any shear layer, where we may not have an explicit parameterization, we also introduce a generic shear thickness parameter Δ. We expect the particular δ of Equation (3) to be proportional to the generic parameter Δ (Figure 1).

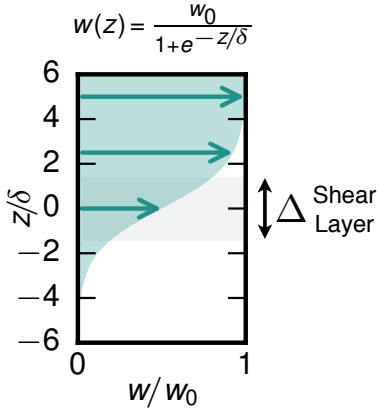

Figure 1. Logistic wind profile.

II. Step wind solution

In the limit of thin shears, Equation (2) simplifies to

$$\mathbf{x}' = \mathbf{f}_0(\mathbf{x}, \mathbf{u}) + \mathbf{f}_1(\mathbf{x})\delta(z) \tag{4}$$

with $\mathbf{x} = [v, \gamma, \psi, z]^T$ and $\mathbf{u} = [c_L, \phi]^T$, and

$$\mathbf{f}_0 = \begin{bmatrix} -c_D v^2 - \sin\gamma \\ c_L v \cos\phi - \cos\gamma / v \\ c_L v \sin\phi / \cos\gamma \\ v \sin\gamma \end{bmatrix}, \quad \mathbf{f}_1 = w_0 \sin\gamma \begin{bmatrix} v\cos\gamma\sin\psi \\ -\sin\gamma\sin\psi \\ \cos\psi/\cos\gamma \\ 0 \end{bmatrix}$$

represent the continuous evolution of the state space on either side of the shear layer $z = 0$, where the wind is uniform, and the discontinuous effect of crossing the shear layer, respectively. $\mathbf{f}_1$ only plays a role when the boundary layer is being crossed, suggesting the special role of the state at that moment. We define $\mathbf{x}_0 = (v_0, -\psi_0, \gamma_0, 0)$ to be the airplane's state when it is up-crossing. The problem of finding the minimum wind for which Equation (2) or (4) have a periodic solution is of particular interest and the topic of this paper.

Note that Equation (2) is invariant by addition of a global constant to the wind field, suggesting that the ground frame of reference does not play any particular role for the minimum wind problem. Instead, we discussed in [1] how the symmetry of the system is increased when analyzed in the Galilean frame of reference that is convected with the average wind.

In [1], we solved the minimum wind problem numerically for various shear thicknesses δ by direct collocation, in a procedure adapted from [12,25]. It was observed that as δ is decreased, the trajectories become more and more 2D as the climb angle amplitude γ_0 decreases to 0.

In the limit of thin shears, the trajectory can therefore be decomposed as a succession of glide phases on either side of, but infinitely close to, the shear layer ($\gamma = 0, z = 0^{\pm}$) and transitions through the shear layer $\mathbf{x}_{\text{new}} = \mathbf{x}_{\text{old}} + \mathbf{f}_1(\mathbf{x}_0)/v_0 \sin\gamma_0$. In fact, in the thin shear limit, both glide phases are equivalent and every "S" can be viewed as the succession of two energetically identical sub-cycles, such that up-crossing

and down-crossing are equivalent. During the glide phases there is an overall loss of airspeed, and at each transition there is an equal and opposite airspeed gain.

The hypothesis that the glide phase is horizontal imposes a condition on the relationship between lift and bank angle $\cos\phi = 1/c_L v^2$ such that Equation (4) can be transformed into

$$\frac{dv}{d\psi} = -\frac{c_D}{c_L}\frac{v}{\sqrt{1-\frac{1}{c_L^2 v^4}}}\,\mathrm{sign}(\psi'). \tag{5}$$

The turn amplitude of each glide phase is $2\psi_0$ such that the airspeed loss is approximately $2\frac{dv}{d\psi}\psi_0$.

With the same hypotheses, the change in airspeed at each transition is $v_{\text{new}} = v_{\text{old}} + w_0 \sin\psi_0$. Finally, equating the airspeed loss during glides and the airspeed gain at transitions we get

$$\frac{2c_D}{c_L}\frac{v}{\sqrt{1-1/c_L^2 v^4}} = \frac{\sin\psi_0}{\psi_0} w_0 \tag{6}$$

which has a minimum airspeed-wind pair

$$v^* = 3^{1/4}/\sqrt{c_L}\ , \quad w^* = \frac{3^{3/4}\sqrt{2}}{c_L^{3/2}/c_D}. \tag{7}$$

Importantly, it is reached when $\psi_0 \to 0$.

This result goes at odds with the generally accepted description of dynamic soaring, in which the airspeed gain is explained by portraying the albatross climbing up facing the wind, or down with the wind. Our new finding can be explained intuitively in the following way: the airspeed gain at each transition is proportional to $\sin\psi_0$, the dot product between the airspeed vector and the wind speed. The airspeed loss during glides is proportional to the angle of turn ψ_0. While airspeed gain in *one single* transition is maximized when the plane is traveling directly facing the wind or away from it, the *ratio* between gains and losses, proportional to $\frac{\sin\psi_0}{\psi_0}$, is maximized in the limit of small turns and frequent transitions. More information and further discussions may be found in [1].

III. Asymptotic expansion for finite thickness

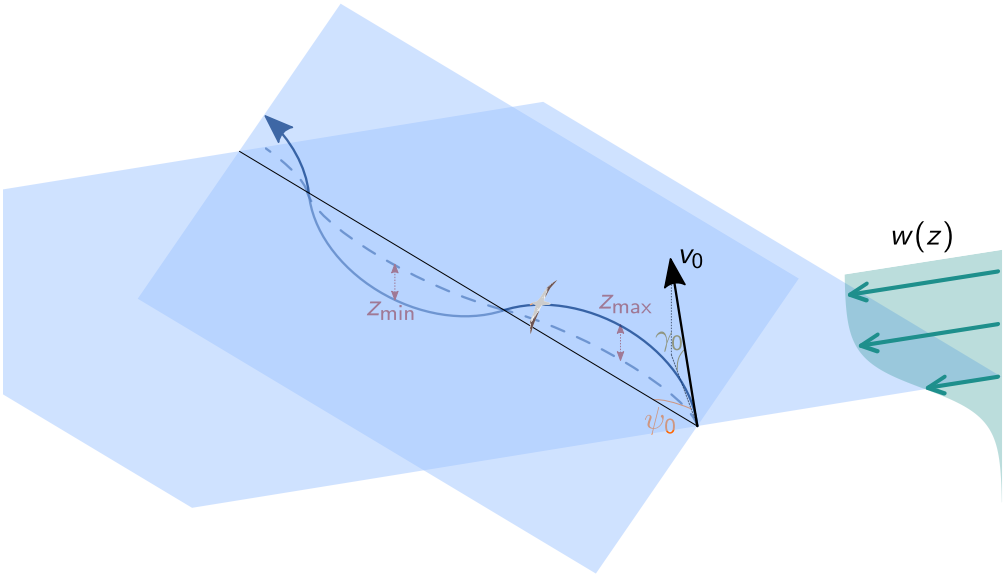

Figure 2. Trajectory in a wind field of finite shear thickness. Following observations from numerical trajectory optimization (Figure 3), we assume that the trajectory lies on a slanted plane.

Even for finite shear thicknesses (up to $\delta \lesssim 1/10$), the numerical solutions show that the trajectories remain essentially planar –though that plane is inclined to the horizontal–, as described in Figure 2. More

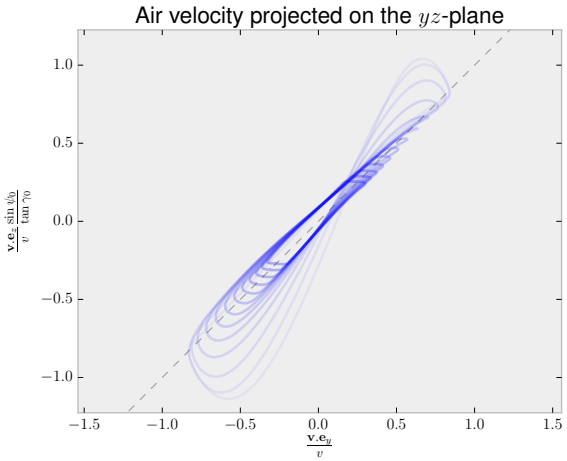

Figure 3. Airspeed vector from trajectory optimization, projected onto the crosswind, yz-plane: each loop represents the evolution of the y and z components of the airspeed vector over one cycle. The lightest color is for $\delta = 1/2$, For each subsequent line the thickness is halved until $\delta = 1/2^{13}$. When δ is small, and especially for the low altitude glide, the velocity vector closely follows a plane of slope $\tan\gamma_0/\sin\psi_0$.

precisely, as Figure 3 shows, the velocity vector closely follows a geometric plane. This plane is generated by the crosswind direction $\mathbf{e}_x$ and the airspeed vector at transition $\mathbf{v}_0 = v_0(\cos\gamma_0\cos\psi_0, \cos\gamma_0\sin\psi_0, \sin\gamma_0)^T$. The planar constraint can be rewritten as

$$\tan\gamma/\sin\psi = \tan\gamma_0/\sin\psi_0,$$

which is a generalization of assumption $\gamma = 0$ used in the previous section. Formally, because of the planar constraint, an algebraic operation similar to that transforming Equation (2) into Equation (5) is possible. After some tedious algebra, we obtain the approximate equation

$$\frac{dv}{d\psi} \approx -\frac{v}{f\sigma}\left(1 + \frac{1}{2\sigma^2}\left(\frac{\gamma_0}{\psi_0}\right)^2\right)\mathrm{sign}(\psi') \tag{8}$$

where $f = c_L/c_D$ and $\sigma = \sin\phi = \sqrt{1 - \frac{1}{c_L^2 v^4}}$. The $\approx$ sign indicates that this equation is a truncated series. Note that Equation (8) converges to Equation (5) for $\gamma_0/\psi_0 \to 0$.

In finite shear thickness, there is an extra drag term due to the fact that flying through the shear layer is associated to a finite distance. The loss in airspeed is approximately

$$\int_{t^-}^{t^+} -c_D v^2 dt \approx \frac{c_D v_0 \Delta}{\sin\gamma_0}$$

where Δ is the thickness of the shear layer.

Equating as in the previous section the airspeed gains and losses, the following approximate relation is obtained:

$$w_0 \sin\psi_0 \cos\gamma_0 = \frac{2v_0\psi_0}{f\sigma}\left(1 + \frac{1}{2\sigma^2}\left(\frac{\gamma_0}{\psi_0}\right)^2\right) + \frac{c_D v_0 \Delta}{\sin\gamma_0}. \tag{9}$$

Note that although for simplicity the focus here is on the purely minimum wind problem, which is crosswind in an *air-relative* sense, the above relation is in fact *directly transformable* to trajectories that are upwind or downwind on average through the simple transformation $w_0 \to w_0\cos\psi_{\text{avg}}$.

Ideally one would solve the following optimization problem

$$\begin{aligned} &\underset{\psi_0,\gamma_0,v_0,c_L}{\text{minimize}} && w_0 \\ &\text{subject to} && \text{Equation (9)}. \end{aligned} \tag{10}$$

Instead in this paper we only minimize with respect to the variables that tend to 0 for thin shears, *i.e.* ψ_0 and γ_0. To the dominant order we obtain

$$\frac{\partial w_0}{\partial \psi_0} = 0 \;\Rightarrow\; \psi_0^3 \gamma_0 = \frac{6 c_D v_0 \Delta}{w^*}, \quad \frac{\partial w_0}{\partial \gamma_0} = 0 \;\Rightarrow\; \gamma_0^3 \psi_0 = \frac{\sigma^2 c_D v_0 \Delta}{w^*}.$$

This may be rewritten as

$$\gamma_0^* = \left(6\sigma^6\right)^{1/10} \left(\frac{c_D v_0 \Delta}{w^*}\right)^{2/5}, \quad \psi_0^* = \frac{6^{3/10}}{\sigma^{1/5}} \left(\frac{c_D v_0 \Delta}{w^*}\right)^{1/5}. \tag{11}$$

Note that $\sigma = \sqrt{2/3}$ when $v = v^*$ (corresponding to a bank angle of 55°, which is consistent with observations of albatrosses). With this, the required wind w_0 in finite shear thicknesses can be recovered by reinjection of γ_0^* and ψ_0^* into Equation (9).

Finally, ψ_0^* and γ_0^* provide an estimation for the vertical distance between the lowest and highest points of the cycle $z_{\text{travel}} = z_{\max} - z_{\min}$ (Figure 2). Indeed, the radius of curvature is given by $r = v^2 \cot\phi$. Analyzed in the plane-of-flight, the arcs of the gliding phases have an angle of amplitude $\cos\theta = \mathbf{v}_0.\mathbf{e}_x/v_0 = \cos\psi_0 \cos\gamma_0$ such that the distance between the trajectory's apex or bottom and the axis $\mathbf{e}_x$ is $d = r(1-\cos\theta)$. The inclination of the plane-of-flight is $\tan\zeta = \mathbf{v}_0.\mathbf{e}_z/\mathbf{v}_0.\mathbf{e}_y = \tan\gamma_0/\sin\psi_0$, such that the apex and bottom altitudes are $z_{\max\,/\,\min} = \pm d \sin\zeta \approx \pm d \tan\gamma_0/\sin\psi_0$. As a result, to the dominant order

$$z_{\text{travel}} \approx \frac{\sqrt{3}}{\sqrt{2} c_L} \psi_0 \gamma_0 \sim \Delta^{3/5}. \tag{12}$$

IV. Validation and discussion

IV.A. Validation against our numerical trajectory optimization

We tested our asymptotic model against the numerically optimized trajectories of [1]. Figure 4 collects the scaling of various quantities from our trajectory optimization as a function of the shear thickness. The fits were performed on shears with $\delta \leq 1/32$. As shown, the asymptotic solution predicts scalings that agree extremely well with trajectory optimization. Figure 5 compares directly the asymptotic model with the trajectory optimization as a function of the shear thickness parameter δ. In order to directly compare the asymptotic expansion with the trajectory optimization, we set $\Delta = 2.2\delta$. This value was chosen by approximately matching z_{travel} in thin shears for the two models (Figure 6).

For $\delta \lesssim 0.1$ the asymptotic model predicts ψ_0, γ_0, w_0 within a 10% of the computationally expensive trajectory optimization. There is a slight over-prediction of the required wind, which is likely in part due to the fact that we have not minimized with respect to v_0 in Equation (10).

Note that the fastest growing error of the model is the prediction of z_{travel}, with a relative error close to 50% at $\delta = 0.1$. In particular, while our model assumes that the trajectory remains planar and up-down symmetric, the numerical results exhibit a strong symmetry break of the trajectory as early as $\delta \sim 10^{-2}$. This is likely due to the fact that for large amplitude up-turns, hammerhead-type trajectories where the glider climbs and stores kinetic energy, is energetically advantageous. Indeed, the turn is then operated at a slower speed and with less drag losses. This remark is consistent with the general form of the loitering trajectory in [1] as well as the trajectory proposed in [11]. However, down-turns remain approximately planar even in thick shears (*c.f.* Figure 3) such that $z_{\min}$ is approximated within 15% even for thick shears $\delta \lesssim 0.1$ and more.

This observation suggests that an important parameter of dynamic soaring is the vertical travel during the down-turn, *i.e.* the difference in altitude between the lowest point of the cycle and the points of zero bank (approximately equal to $|z_{\min}|$ both in the present asymptotic expansion and [1]). Furthermore, this implies that the generalization of γ_0, ψ_0 to more complex models should be the pitch and heading *at the time of zero bank angle*. Figure 7 shows that indeed when expressed as a function of $z_{\min}$, the asymptotic expansion and trajectory optimization agree within 20% or better up to $2z_{\min} \approx 1$ *i.e.* $\delta \approx 0.1$. Note that for albatrosses, $0.25 \lesssim 2z_{\min} \lesssim 1$. Note also that while Figure 5 is obtained after adjusting the ratio Δ/δ, Figure 7 does not. Instead, it relates observable aspects of the trajectory together, without explicitly relying on the wind parameterization, in essence "abstracting away" the specifics of the wind profile. In [1] we hypothesize that the main features of the wind profile, but not its exact shape, should capture the majority of the dynamic

soaring cycle. If this is indeed the case, Figure 7 should be a good approximation of dynamic soaring in other wind fields, such as logarithmic or power-law profiles as well as real ocean winds, and perhaps even of turbulence soaring.

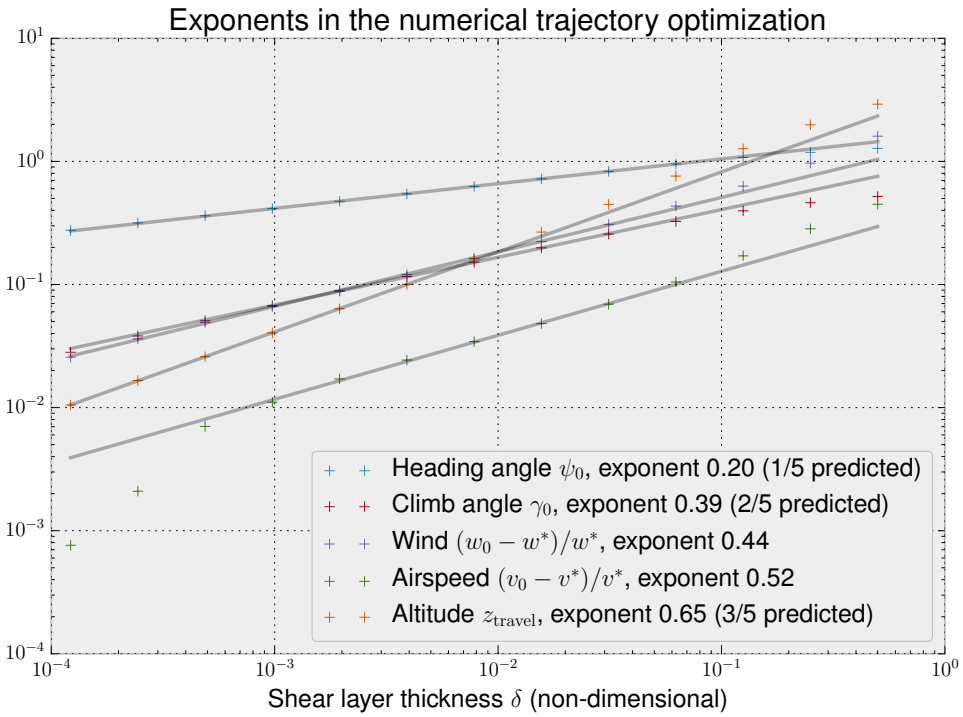

Figure 4. Least-square log fit of the quantities of interest from the numerical optimization in [1], as a function of the shear thickness parameter δ. For each variable, the exponent obtained by least-square fit is indicated in the legend. The asymptotic expansion of equations (11) and (12) predicts scalings that agree extremely well with the numerical trajectory optimization.

IV.B. Validation against trajectory optimizations in logarithmic and power-law wind profiles

[5, 6] simulate a glider of cruise speed $V_c = 15$m/s ($\lambda = 22$ m) and $(c_L^{3/2}/c_D)_{\max} = 24$ in a power-law profile representative of an oceanic wind. They find an minimum-wind trajectory that requires a 3.8 m/s wind speed difference between its highest and lowest points. In [5] $z_{\min} \approx 7$ m. Again, this represents the altitude difference between the lowest point of the trajectory and the altitude of zero bank angle. The solution is reported in Figure 7. Despite the difference in wind and dynamic model with the present study, all predictions for the minimum wind are within 25% of each other. Note that Sachs sets a $c_{L,\max}$ constraint in his dynamic model, which [1] does not have.

[12] consider a glider with a smaller wing loading $V_c = 8.2$ m/s flying in a log profile. They compare three levels of airplane modeling complexity. Their results are reported in Figure 7. Again, our analytic expansion agrees with their results within 20% or less for all quantities of interest. In fact, the variability between their models is of the same order as the variability with respect to the present asymptotic expansion.

Overall, as noted in [6, 12] the uncertainty is dominated by how close to the surface the glider can go and how well it is able to embed itself inside the slow boundary layer.

IV.C. Validation against recordings of flying albatrosses

While quantitative data for albatrosses remains scarce (in particular the recent published recordings provide very little altimetric data), [4, 9, 10] suggest that in the lighter winds, the wandering albatross' trajectory is typically 8-10 m high and reaches higher altitudes in higher winds, *i.e.* $z_{\min} \sim 4$ m. Data from Figure 11 in [10] are included in Figure 7. This data was chosen because the wandering albatross is reported to perform dynamic soaring in winds of 7+ m/s, close to the wind speed of that recording. We utilize a typical wing loading values for the wandering albatross[5] with $V_c = 14.5$ m/s, *i.e.* $\lambda = 22$ m, and assume that the albatross

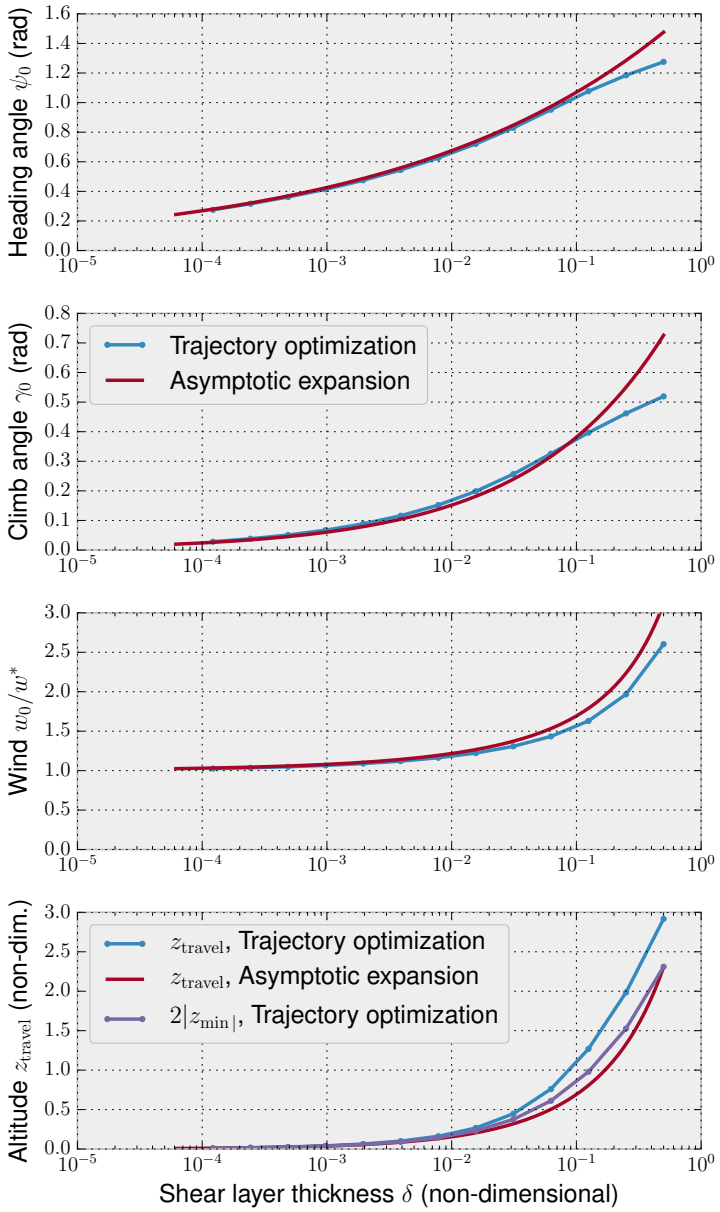

Figure 5. Comparison between the numerical trajectory optimization in [1] and the asymptotic expansion in equations (9) and (11).

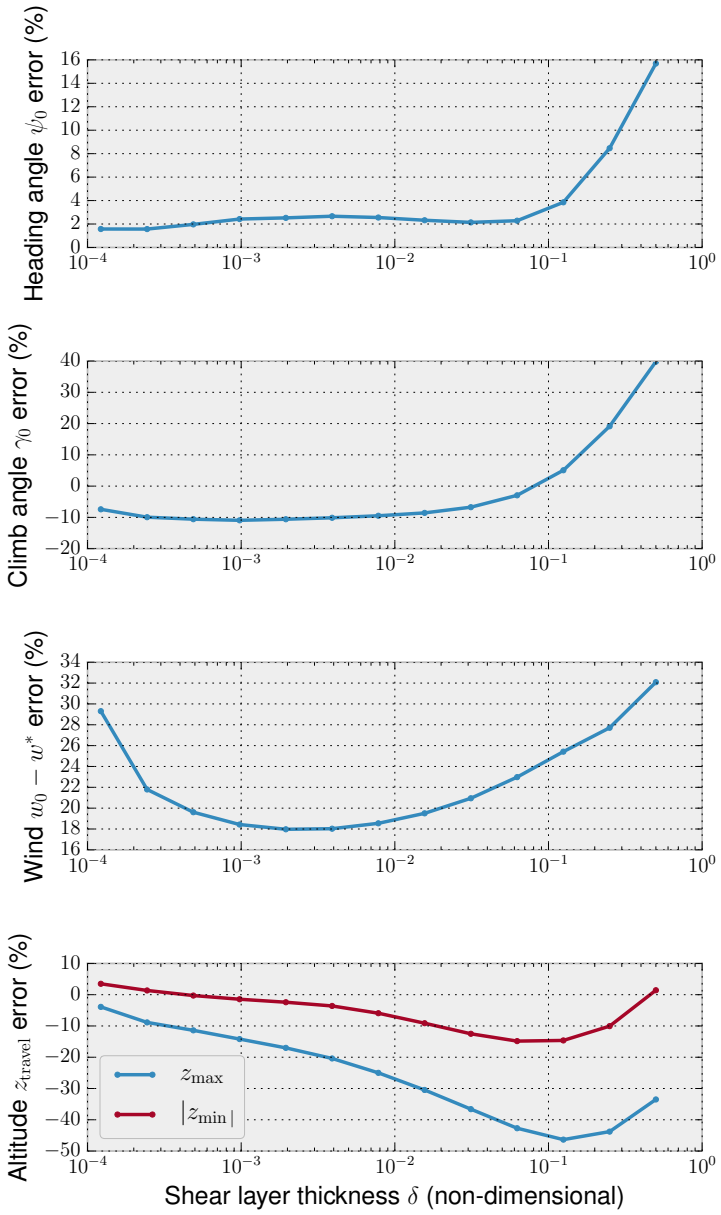

Figure 6. Percentage error between asymptotic expansion in in equations (9) and (11) and the numerical trajectory optimization in [1]. For each quantity x, $(x_{\text{asympt. expans.}} - x_{\text{traj. opt.}})/x_{\text{traj. opt.}}$ is displayed. The asymptotic expansion predicts the heading and climb angle amplitudes within 3% and 10% respectively for $\delta \lesssim 0.1$. In that same range of δ, the *change in wind from the $\delta = 0$ limit* is predicted within $\sim 25\%$. The prediction on the *wind* itself (not plotted) is accurate within less than 10%. Finally the trajectory lowest and highest altitudes are the least well captured parameters, with errors up to 15% and 45% respectively.

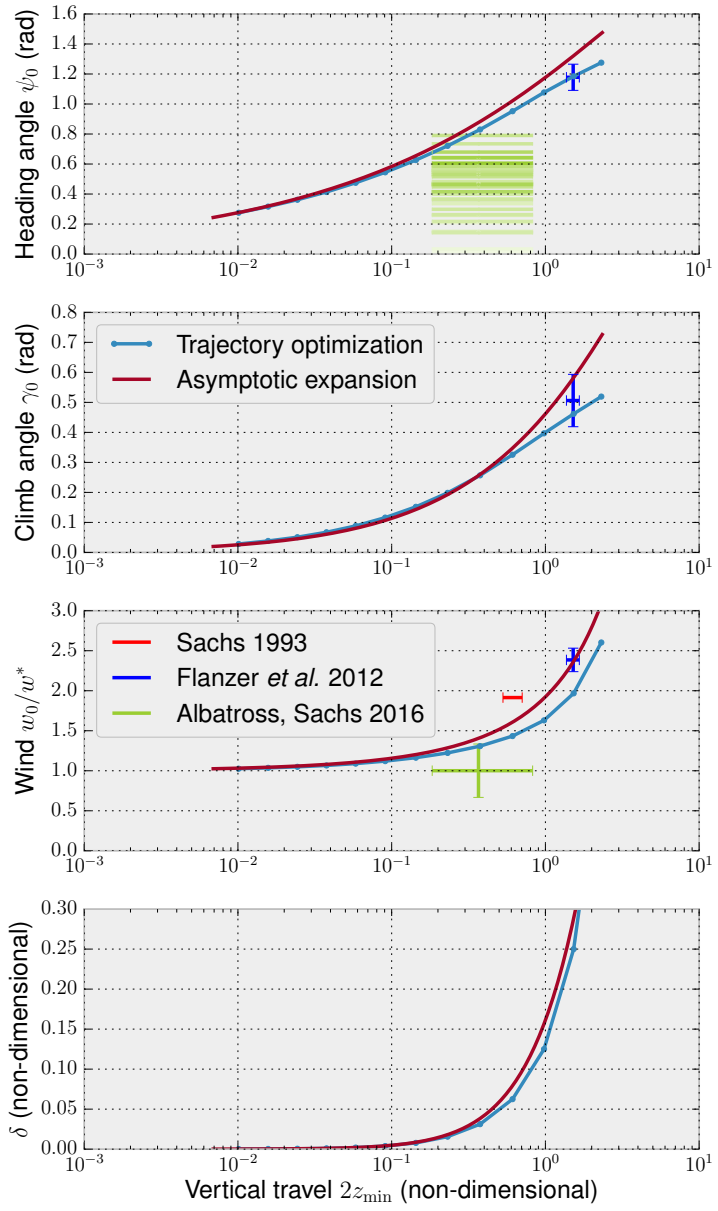

Figure 7. Comparison between the numerical trajectory optimization in [1], the asymptotic expansion in equations (9) and (11), numerical trajectory optimization in logarithmic fields from the literature[5,12] (red and blue), and albatross flight data[10] (green) as a function of the vertical travel during the lower turn. In the first plot, the horizontal green lines represent the individual turns of an albatross flying in a 7.8 m/s wind, reported in Figure 11 of [10] (the color intensity codes the length of the turns). For the quantities of interest, the minimum wind trajectories in logistic and logarithmic wind profiles are similar within 25% or less, indicating the large applicability of approximating the wind field by its intensity and shear layer thickness. The albatross' flight on this recording is also qualitatively well captured, with indications that it may 1) turn less than if purely following a minimum wind trajectory, and 2) efficiently harvest the wind energy, possibly also utilizing mechanisms not included in the present model.

utilizes 25-50% of the wind speed at 10m. The heading of the groundspeed is used as an estimate of ψ_0. It is interesting to note that the albatross seems to turn less than what our model predicts for the minimum wind trajectory.

V. Conclusion

In [1] we discussed how the minimum wind trajectories depend strongly on the shear layer thickness (*i.e.* the distance between the calm and windy layers) and showed that in the limit of thin shear, the optimal trajectory is a succession of small amplitude arcs nearly crosswind, rather than a sequence of half-turns.

In this paper we extend [1] by formulating an asymptotic solution for small but finite shear thicknesses. Our formulation relies on the key assumption, backed-up by observation of the numerical trajectory optimization from [1], that even in finite shears the minimum wind trajectory remains approximately planar. Our asymptotic expansion provides an analytic approximation to key parameters of the minimum wind dynamic soaring cycle, such as heading angle amplitude, climb angle, cycle altitude, and required wind. Its predictions agree within ∼15-25% with numerical models that take seconds or minutes to run on a modern desktop computer. We anticipate that our model will provide a better physical understanding of dynamic soaring, and constitute the basis for efficient and accurate model reduction, with applications both in engineering and in biology. Furthermore, dynamic soaring can also be viewed as a deterministic proxy for turbulence soaring, and our results and techniques are likely extensible in this direction.

Finally, a field that could particularly benefit from these results if that of online trajectory planning, be it at the single cycle scale or at the mesoscale. Indeed, approximate dynamic programming techniques may succeed or fail depending on whether or not a good heuristics is available. Our model might be a step in that direction.

VI. Acknowledgements

The authors wish to thank J.S. Izraelevitz for thoughtful discussions and comments. G. B. acknowledges partial funding from the Link Foundation Fellowship.

References

[1]Bousquet, G. D., Triantafyllou, M. S., and Slotine, J.-J. E., "Asymptotic Solution to the Rayleigh Problem of Dynamic Soaring," *arXiv*, 2016.

[2]Patel, C. K., Lee, H.-T., and Kroo, I. M., "Extracting Energy from Atmospheric Turbulence," *XXIX OSTIV Congress*, Lüsse-Berlin, Germany, 2008.

[3]Rayleigh, J. W. S., "The Soaring of Birds," *Nature*, Vol. 27, 1883, pp. 534–535.

[4]Idrac, P., "Étude expérimentale et analytique du vol sans battements des oiseaux voiliers des mers australes, de l'Albatros en particulier," *La technique aéronautique : revue des sciences appliquées à la locomotion aérienne*, Vol. 16, 1925.

[5]Sachs, G., "Minimaler Windbedarf für den dynamischen Segelflug der Albatrosse," *Journal für Ornithologie*, Vol. 134, 1993, pp. 435–445.

[6]Deittert, M., Richards, A., Toomer, C. A., and Pipe, A., "Engineless Unmanned Aerial Vehicle Propulsion by Dynamic Soaring," *Journal of Guidance, Control, and Dynamics*, Vol. 32, No. 5, sep 2009, pp. 1446–1457.

[7]Bower, G., *Boundary Layer Dynamic Soaring for Autonomous Aircraft: Design and Validation*, Ph.D. thesis, Stanford University, 2011.

[8]Richardson, P. L., "How do albatrosses fly around the world without flapping their wings?" *Progress in Oceanography*, Vol. 88, No. 1-4, 2011, pp. 46–58.

[9]Sachs, G., Traugott, J., Nesterova, A. P., Dell'Omo, G., Kümmeth, F., Heidrich, W., Vyssotski, A. L., and Bonadonna, F., "Flying at No Mechanical Energy Cost: Disclosing the secret of Wandering Wlbatrosses." *PLOS one*, Vol. 7, No. 9, jan 2012.

[10]Sachs, G., "In-flight measurement of upwind dynamic soaring in albatrosses," *Progress in Oceanography*, Vol. 142, 2016, pp. 47–57.

[11]Hendriks, F., *Dynamic Soaring*, Ph.D. thesis, UCLA, 1973.

[12]Flanzer, T. C., Bunge, R. A., and Kroo, I. M., "Efficient Six Degree of Freedom Aircraft Trajectory Optimization with Application to Dynamic Soaring," *AIAA Aviation Technology, Integration, and Operations Conference*, Indianapolis, Indiana, 2012.

[13]Bonnin, V., *From Albatrosses to Long Range UAV Flight by Dynamic Soaring*, Ph.D. thesis, University of the West of England and ISAE, 2016.

[14]Pennycuick, C. J., "The Flight of Petrels and Albatrosses (Procellariiformes), Observed in South Georgia and its Vicinity," *Philosophical Transactions: Biological Sciences*, Vol. 300, No. 1098, 1982, pp. 75–106.

[15]Boslough, M. B. E., "Autonomous Dynamic Soaring Platform for Distributed Mobile Sensor Arrays," Tech. rep., Sandia National Laboratories, 2002.

[16]Lissaman, P., "Wind Energy Extraction by Birds and Flight Vehicles," *AIAA Guidance, Navigation, and Control Conference*, Reno, Nevada, 2005.

[17]Barate, R., Doncieux, S., and Meyer, J.-A., "Design of a bio-inspired controller for dynamic soaring in a simulated unmanned aerial vehicle." *Bioinspiration & biomimetics*, Vol. 1, No. 3, 2006, pp. 76–88.

[18]Denny, M., "Dynamic soaring: aerodynamics for albatrosses," *European Journal of Physics*, Vol. 30, No. 1, jan 2009, pp. 75–84.

[19]Lawrance, N. R. J., *Autonomous Soaring Flight for Unmanned Aerial Vehicles*, Ph.D. thesis, University of Sidney, 2011.

[20]Bonnin, V. and Toomer, C. C., "Energy-Harvesting Mechanisms for UAV Flight by Dynamic Soaring," *AIAA Guidance, Navigation, and Control Conference*, Boston, MA, 2013.

[21]Bird, J. J., Langelaan, J. W., Montella, C., Spletzer, J. R., and Grenestedt, J. L., "Closing the Loop in Dynamic Soaring," *AIAA Guidance, Navigation, and Control Conference*, National Harbor, Maryland, 2014.

[22]Gao, X.-Z., Hou, Z.-X., Guo, Z., and Chen, X.-Q., "Energy extraction from wind shear: Reviews of dynamic soaring," *Proceedings of the Institution of Mechanical Engineers, Part G: Journal of Aerospace Engineering*, Vol. 229, No. 109, 2015, pp. 2336–2348.

[23]Zhao, Y. J., "Optimal patterns of glider dynamic soaring," *Optimal control applications and methods*, Vol. 25, No. 2004, 2004, pp. 67–89.

[24]Buckley, M. P. and Veron, F., "Structure of the Airflow above Surface Waves," *Journal of Physical Oceanography*, Vol. 46, No. 5, 2016, pp. 1377–1397.

[25]Hargraves, C. R. and Paris, S. W., "Direct Trajectory Optimization Using Nonlinear Programming and Collocation," *AIAA J. Guidance*, Vol. 10, No. 4, 1987, pp. 338–342.